ELSEVIER

Contents lists available at ScienceDirect

Applied Thermal Engineering

journal homepage: www.elsevier.com/locate/ate



Research Paper

Digital twin development of a full-scale industrial heat pump

Ali Can Ispir a , Gustavo Otero Rodriguez b, Wouter de Vries b, Michel Speetjens a

- ^a Eindhoven University of Technology (TU/e), Department of Mechanical Engineering, PO Box 513, 5600 MB, Eindhoven, The Netherlands
- b Netherlands Organisation for Applied Scientific Research (TNO), Sustainable Technologies for Industrial Processes, Energy & Materials Transition Unit, P.O. Box 15 1755 ZG Petten, The Netherlands

ARTICLE INFO

MSC: 00-01 99-00

Keywords:
Digital twin
Waste-heat recovery
Heat pump
Natural refrigerant
Machine learning
Experimental study

ABSTRACT

Industrial heat pumps (HPs) are a sustainable alternative to fossil-fueled boilers for process heat generation, particularly when powered by green electricity. However, their wider adoption is hindered by a limited understanding of HP performance under diverse operating conditions. Traditional methods for studying HP performance, such as high-fidelity numerical simulations or experimental testing, are often costly and impractical. To address this, we propose a digital-twin framework that unites machine learning, specifically Gaussian Process Regression (GPR), to efficiently model an industrial HP for energy recovery from (industrial) waste heat using experimental data. This approach is novel, as few data-driven models have been developed for designing industrial HPs employed for this purpose, thereby contributing to achieving a sustainable processing industry. This digital twin was developed for a 1 MWth industrial HP, using n-Pentane as the working medium and recovering waste heat from hot water to produce steam for industrial processes, and trained by experimental data collected from 55 steady-state operating points in a state-of-the-art test facility. The digital twin accurately predicts both relevant process variables (e.g. outlet pressures and temperatures) for each HP component and key performance indicators, including the Coefficient of Performance (COP) and heating duty, with prediction errors within 7% as a function of process parameters such as flow properties of the hot-water source, compressor rotational speed, and steam pressure. The digital twin is furthermore applied for an economic and environmental analysis, demonstrating a payback period of 3.8-4.2 years and reductions in CO₂ emission of 250-1000 tons annually compared to a propane-fueled boiler. The HP achieved a COP equal to 44% of the Carnot COP based on condenser/evaporator saturation temperatures and enabled significant energy savings, exceeding 3000 MWh annually when operated at steam pressures of 1.9-2.4 bar. This study hereby demonstrates the potential of data-driven models to enhance the design and operation of industrial HPs and thus provides an efficient and scalable framework for developing and advancing sustainable energy systems in industry.

1. Introduction

Industrial processes in the European Union account for approximately 26% of final energy consumption [1] and nearly 20% of total greenhouse gas (GHG) emissions [2]. Currently, industries such as food processing, paper production, and refineries primarily rely on fossilfuel-powered boilers for their heat supply. Industrial heat pumps (HPs) offer a promising alternative for reducing GHG emissions in processes requiring low-temperature heat (<200 °C), resulting in an increase in market interest [3]. Unlike boilers, HPs can recycle and amplify energy in a potentially sustainable manner: by utilizing waste-heat from the processes and consuming one unit of (renewable) electricity, HP can

produce three to four units of heat at the desired temperature for an industrial process. The prevalent HP technology involves the closed-cycle vapor compression cycle, initially developed for refrigeration and now adapted to heating [3]. Despite their potential, significant challenges impede the widespread adoption of industrial HPs. A major barrier is end-user uncertainty about adding new equipment (e.g. an HP) that could disturb their production process [3]. A potential solution to overcome such end-user uncertainty is to demonstrate the HP performance across a wide range of operating conditions typical in industrial settings via accurate predictions. Traditional methods, such as high-fidelity numerical and experimental analyses, are prohibitively expensive and impractical [4]. Conversely, low-fidelity approaches such as reduced-order modeling often fail to estimate a HP system performance due

E-mail address: a.c.ispir@tue.nl (A.C. Ispir).

^{*} Corresponding author.

 ΔP

λ

σ

Σ

φ

ω

NL

Subscripts

Nomenclature	
Acronyms	
COD	Coefficient of Determination
COP	Coefficient of Performance
GPR	Gaussian Process Regression
HP	Heat pump
ML	Machine learning
MVN	Multi-variate normal
Variables	
A	Area [m ²]
E	Energy [MW]
h	Specific enthalpy [kJ/kg]
m	Mass flow rate [ton/h]
\mathcal{N}_D	Multi-variate normal (MVN) distribution
P	Pressure [bar]
PBT	Payback time [year]
Q	Heat exchange [kW]
R^2	Coefficient of Determination (COD)
t	Duration [h/year]
T	Temperature [°C]
\dot{V}	Volumetric flow rate [m ³ /h]
W	Compressor electric power consumption [kW]
x	Independent variable/data point
x_*	Interpolation point
y	Dependent variable

Pressure drop [bar] Efficiency

Standard deviation

Covariance matrix

Conversation factor

Related to the Netherlands

Compressor rotational speed [r/min]

Price [€]

to the complexity of HP geometry and physical processes. To fill the gap between such low-fidelity and high-fidelity approaches, several studies have focused on developing suitable digital twins to estimate and predict HP performance under design and off-design operational conditions. The present study aims to contribute to these efforts.

An increasingly popular approach for developing digital twins for energy systems and HPs involves data-driven models using machine learning (ML) methodologies based on operational data [5,6]. Evens and Arteconi [7] developed a digital twin for a water/water heat pump of a residential single-family building using long short-term memory (LSTM) neural networks trained by experimental data. This achieved accurate prediction of HP behavior such as electrical power consumption (±10% for 79.70% of the time), condenser outlet temperature ($\pm 1\%$ for 83.89% of the time) and flow rate ($\pm 10\%$ for 89.81% of the time). This study found LSTM neural networks essential for reliable multi-step ahead predictions. The modeling approach was also evaluated for different heating configurations and revealed potential for a broad range of applications. Vering et al. [8] introduced the ReCaMo (repeated calibration or on-line recalibration of simulation models) framework, specifically designed for the continuous calibration of digital twins for HP systems. The framework employs IoT-based communication to update the digital twin with real-time data, enhancing its accuracy over time. The ReCaMo framework, using one month of field data, achieved a prediction error of less than 1 K for the HP supply temperature, demonstrating its potential for operational optimization and predictive maintenance. Butean et al. [9] integrated a digital-twinning approach into a high-temperature HP system that

recuperates heat from a waste-heat source in industrial renewable energy systems. Their method involves analyzing a large amount of real-time HP data and generating digital twins to gain insights into the process using artificial intelligence algorithms. Seifert et al. [10] proposed a digital-twinning framework for HPs, including numerical cycle modeling, utilizing grey-box models for each component, including the control unit, and validated with an experimental setup. Shin and Cho [11] evaluated several ML algorithms to predict the Coefficient of Performance (COP) of an air-to-air HP system under varying sink and source temperatures. They found that artificial neural networks (ANNs) performed the best by establishing accurate relationships between independent and dependent variables with a mean bias error of 3.6%. Wang et al. [12] proposed an ML-based digital twin for an HP in electric vehicles, integrating support vector regression (SVR) with an experimental database of an HP using R134a as the working medium. This digital twin predicted the COP based on indoor and outdoor temperatures, indoor air mass flow rate, compressor speed and expansion valve position, achieving a relative error of 8.5%. Zhang et al. [13] assessed three similar ML-based digital twins to predict the COP of groundsource HPs using various input parameters such as heat-exchanger inlet and outlet temperatures, mass-flow rates, relative humidity, and indoor temperature. They found that, among the considered ML approaches, the Extreme Learning Machine algorithm performed the best. The recent study on predicting the COP in refrigeration systems by Zhou and Zhu [14] developed a digital twin that combines convolutional neural networks (CNN), multilayer perceptrons (MLP), and LSTM networks. This included real-time optimization of the model parameters by Particle Swarm Optimization to minimize the difference between the physical and predicted COP. Their digital-twinning approach outperformed individual methods such as CNN. Aguilera et al. [15] proposed a digital twin of a two-stage HP system based on real-time HP operational data for determining optimal intermediate pressure set points at different levels of fouling. The digital twin enabled estimating the optimal intermediate pressure, improving the COP up to 3%, as well as quantifying the effects of fouling by the thermal resistance and pressure drop in the HP components. Lv et al. [16] introduced a digitaltwinning approach for an air-conditioning system in a train station in Xichang, China by combining fuzzy (c + p) means clustering (FCPM) with the stacked broad learning system (SBLS) algorithm (FCPM-SBLS) algorithm. This resulted in accurate COP predictions.

The aforementioned efforts significantly contributed to data-driven ML-based HP modeling. However, similar studies focusing on HPs used for waste-heat recovery and heat recuperation in industrial applications (especially operating with natural working media) are scarce to date due to the limited availability of experimental data suitable for ML-based digital twinning. Our study therefore concentrates on developing digital twins for such HP applications from experimental data.

Developing data-driven HP models typically relies on databases built from experimental measurements or high-fidelity numerical simulations. Experimental testing of high-temperature HPs is generally scarce. Jian et al. [17] reviewed 15 experimental studies of prototype or small-scale HPs that deliver heat above 130 °C and highlighted the most relevant ones for this application area. Marina et al. [18] tested a two-stage steam-producing industrial HP using pentane, with a thermal capacity of 150 kWth, generating 4.8 barA steam with a temperature lift of 90 °C. Liu et al. [19] investigated a 70 kWth compression-absorption HP prototype using ammonia-water and producing high-temperature steam at 150 °C. Pan et al. [20] tested a water-to-water HP below 100 °C for various working medium, including mixtures. Navarro et al. [21] examined a high-temperature HP operating on R-1336mzz(Z), delivering heat at 155 °C with a heating capacity of around 10 kW using a scroll compressor. Verdnik et al. [22] tested an n-butane HP capable of producing around 30 kWth of heat at 110 °C in subcritical and 160 °C in transcritical operation. Ramirez et al. [23], both experimentally and numerically, investigated a high-temperature steam-producing HP running on R1233zd(E); this prototype includes an external sub-cooler to separate sensible and latent heat production, delivering steam up to 150 °C at 40 kWth. However, none of these high-temperature HPs were experimentally tested at an industrial scale or modeled by a digital twin, both of which are crucial for validating their performance and reliability in real-world applications and for reducing end-user uncertainties about the technology. This is an important motivation for our study.

The present study proposes a data-driven, ML-based digital twin of a 1 MWth steam-producing HP using n-pentane (R601) as the working medium. Gaussian Process Regression (GPR), successfully employed to process HP data before [24,25], is applied to HP data obtained from a full-scale experimental setup at the Carnot Laboratory of the Netherlands Organisation for Applied Scientific Research Center (TNO). The HP is designed to recover waste-heat from hot water at 90 °C to produce steam above 140 °C for industrial processes such as paper and food production. The system includes a screw-type compressor, a condenser (transferring the heat for steam generation), an internal heat exchanger, twin evaporators (identified as evaporators A and B) consuming the (process') waste heat, and an economizer. The behavior and performance of the HP are measured at 55 steady-state operating points, considering various input conditions such as water inlet temperature, volumetric flow rate of the hot water compressor rotational speed, and steam pressure. GPR is applied to these measurement data to create a digital twin that predicts relevant process variables such as e.g. outlet pressures and temperatures, compressor outlet flow conditions and electrical power consumption. These predictions are then used to calculate key performance indicators such as the COP and heating duty (i.e., heat production for steam generation). The digital twin is employed to create performance maps showing the COP, heating duty, and compressor electric power consumption as a function of the process inputs. Furthermore, an economic and CO2 emission analysis is carried out to compare the HP with a boiler for a potential industrial application in the Netherlands.

The structure of this paper is as follows. Section 2 presents the methodology including the performance indicators, the experimental setup, the digital-twinning approach, and the economic and environmental assessment. Section 3 discusses the experimental analysis, the validation of the HP digital twin, and finally, the application of the digital twin to an industrial scenario. Concluding remarks are in Section 4.

2. Methodology

2.1. Performance indicators

The performance of the HP is assessed by the COP, defined as

$$COP = \frac{\dot{Q}_{heating}}{\dot{W}_{comp,electric}},\tag{1}$$

with $\dot{W}_{comp,electric}$ the electric power consumption of the compressor and

$$\dot{Q}_{heating} = \dot{m}_{comp,out} \cdot (h_{condenser,hot,in} - h_{condenser,hot,out}) \cdot \frac{1000}{3600},$$
(2)

the heating duty, i.e., the heat transferred within the condenser from the working medium (condenser hot side) to an external stream (condenser cold side). In this study the heating duty is employed for steam generation and the external stream therefore consists of water that enters the condenser as a saturated liquid and leaves as superheated steam. The inputs for calculating $\dot{Q}_{heating}$ include the mass flow rate $(\dot{m}_{comp,out})$ of the working medium, the compressor outlet pressure ($P_{comp,out}$), and the compressor outlet temperature ($T_{comp,out}$). The enthalpy $h_{comp,out} = h_{condenser,hot,in}$ is determined from $P_{comp,out}$ and $T_{comp,out}$ assuming a superheated state that the compressor outlet. Furthermore assuming negligible pressure drop on the condenser hot side ($P_{condenser,hot,in} = P_{condenser,hot,out}$) and saturated liquid conditions at its outlet, the enthalpy $h_{condenser,hot,out}$ is determined entirely by $P_{comp,out} = P_{condenser,hot,in}.$ The actual COP (1) is bounded by theoretical limits following

$$COP \leq COP_{int} \leq COP_{ext},$$
 (3)

$$COP_{int} = \frac{T_{h,int}}{T_{h,int} - T_{c,int}}, \qquad COP_{ext} = \frac{T_{h,ext}}{T_{h,ext} - T_{c,ext}}, \tag{4}$$

the Carnot COPs based on the internal temperature levels $T_{h,int}$ (condenser saturation temperature) and $T_{c,int}$ (evaporator saturation temperature) and the external temperature levels $T_{h.ext}$ (inlet temperature of the external stream in the condenser) and $T_{c,ext}$ (inlet temperature of the hot water in the evaporator). Defining the Carnot COPs (3) enables evaluation of the actual performance according to COP (1) relative to ideal thermodynamic conditions in terms of the fractions

$$COP_{int}^* = \frac{COP}{COP_{int}} \times 100\%, \qquad COP_{ext}^* = \frac{COP}{COP_{ext}} \times 100\%.$$
 (5)

representing the degree to which the HP achieves the Carnot COPs (4). Fraction $COP_{int}^* \leq 100\%$ reflects to what extent the performance of the HP itself approaches ideal conditions; fraction $COP_{ext}^* \leq 100\%$ reflects to what extent the total performance, i.e., internal performance and thermal interaction with heat source (here: hot water) and heat sink (here: external stream for steam generation) combined, approaches ideal conditions. Note that (3) implies $COP_{ext}^* \leq COP_{int}^* \leq 100\%$.

2.2. Experimental setup

2.2.1. System description

The industrial HP considered in this study is part of the TNO FUSE project [26] and was designed and constructed by Mayekawa Europe [27]. It is a 1 MWth pentane HP, designed to upgrade hot water at 90 °C to produce steam at 140 °C. The HP operates on a closed-cycle vapor compression system, specifically a Reverse Rankine (RR) cycle with an economizer, as depicted in Fig. 1. According to the conceptual design, the working medium (pentane) evaporates at 80 °C and condenses at 145 °C. The heat pump was tested in the dedicated test rig in the TNO Carnot Laboratory [28], which is capable of simulating waste-heat supply and process-heat delivery through a hot-water stream and low-pressure steam generation, respectively.

The HP features a Mayekawa 250MFC screw compressor, custommade by Mayekawa Japan [29], with a swept volume of 2010 m³/h at 3000 RPM and an L-port configuration (fixed Vi of 2.63). It is powered by a Siemens SIMOTICS motor with a capacity of 500 kW at 400 V. An internal heat exchanger (subcooler/superheater), as shown in Fig. 1, ensures that pentane enters the compressor as superheated vapor, preventing droplet formation during compression.

The economizer - an Alfa Laval heat exchanger with a heat transfer area of 12.8 m² - creates three pressure levels in the compressor (suction, intermediate, and discharge) enhancing overall performance by reducing the compressor's workload. This is achieved by splitting the pentane flow post-condenser into two streams: one stream expands to intermediate pressure and evaporates in the economizer heat exchanger, using sub-cooled heat from the other stream, which expands to evaporating (low) pressure. This reduces the amount of working medium compressed from low to high pressure, improving efficiency while maintaining the heating duty.

The condenser of the HP, which serves as a steam generator, is a Caloperm plate-and-shell heat exchanger with a heat transfer area of 78.75 m². On the shell side, water serves as the heat sink, while pentane condenses between the plates. Steam is generated by maintaining a constant water level on the shell side; the water level is maintained using a feedwater pump. Heat transfer occurs as pentane condenses between the plates, transferring heat to the water. Once the water reaches its boiling point, steam is produced. The pressure in the steam generator is regulated by a control valve located in the line leading to

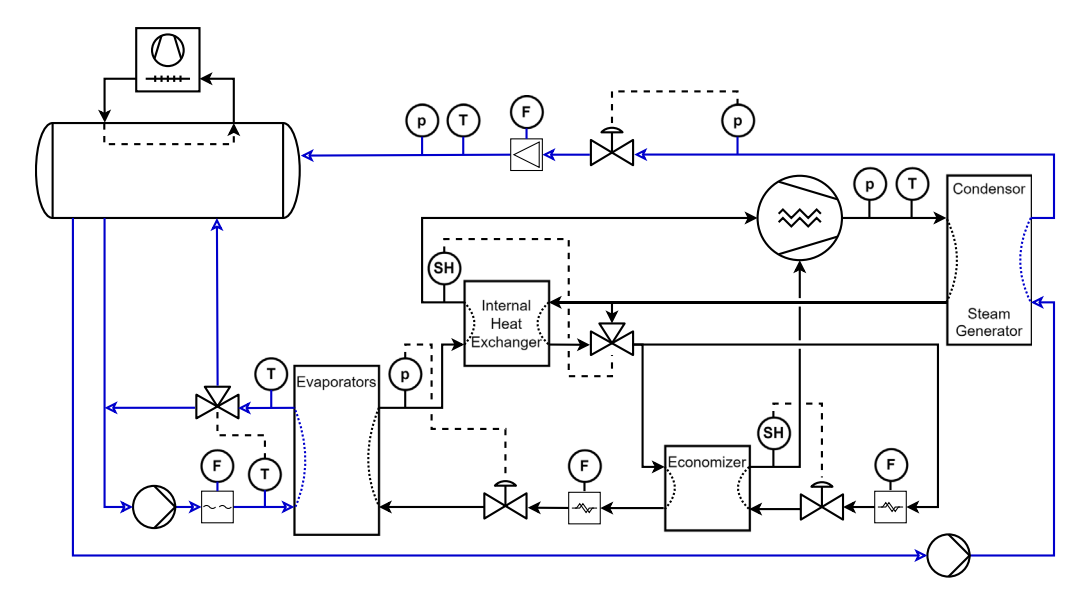


Fig. 1. Simplified schematic overview of TNO HP and test infrastructure (black arrows: pentane flow; blue arrows: condensate/steam flow). The sensor symbols denote F for flow, T for temperature, p for pressure and SH to indicate a calculated superheat based on a combined pressure and temperature measurement.

the buffer vessel of the test rig. Excess heat from the system is rejected to the ambient via a dry cooler.

The system also includes two Alfa Laval brazed plate evaporators, each with a heat transfer area of 67.36 m², operating with direct expansion of pentane. Additional components a Fisher ED DN50 main expansion valve and a Fisher EZ DN25 economizer expansion valve. A Danfoss FC-102 variable frequency drive, rated at 500 kW, provides control and power to the system.

As mentioned, the test rig at the TNO Carnot Laboratory [28] was used to simulate waste heat supply and process heat delivery. This facility supports testing of HP units ranging from 100 kW to 2 MW under various temperature and load conditions. The waste heat temperature ran between 40 °C to 120 °C, with a maximum flow rate of 100 m³/h per evaporator circuit. Steam production reached up to 2570 m³/h, measured using a Krohne OPTISWIRL 4200 C DN150 flowmeter, at pressures ranging from 0.2 bar(g) to 15 bar(g), and a maximum superheated steam temperature of 200 °C. Feedwater temperature was maintained at the saturation temperature of the buffer vessel, and dry cooling was achieved with a 600 kW system at 25 °C ambient temperature. The test rig is equipped with two 40 kW electrical heaters in the buffer vessel to bring the system up to temperature. Finally, the TNO Carnot Laboratory is able to provide an electrical connection of 1 MW at 400 V (1440 A). Fig. 2 shows the Carnot Lab, featuring the tested industrial HP (front) and the test rig (back).

2.2.2. Experimental workflow

After startup, the heat pump and test infrastructure were allowed to stabilize before measurements commenced. This stabilization phase ensured that all components of the system achieved thermal and operational equilibrium. Specifically, the buffer vessel was heated to 105 °C, and the control loops for key parameters - such as evaporator water feed temperature, flow rate, and suction superheat - were engaged to maintain steady conditions. Each measurement represented the average of a 20-min or longer period, during which key operating parameters were closely monitored. In cases of any system instability or upsets, the affected data was discarded, and the system was reset to restore stable operating conditions. This rigorous approach ensured the reliability and repeatability of the experimental data. The buffer vessel held approximately 8 m³ of water, electrically heated to 105 °C before starting the HP. On the waste-heat side, a pump maintained flow by replacing a fraction of cold water returning from the evaporator with hot condensate from the buffer vessel via a three-way valve.

Control loops, as depicted by the dashed lines in Fig. 1, maintained stability throughout the experimental campaign. Key control parameters included:

- Evaporator water feed temperature: Adjusted according to the test point, representing waste heat temperature.
- Water feed flow rate: Maintained at approximately 68 m³/h per evaporator.
- Evaporator pentane pressure: Set to a saturation temperature about 10 K below the water feed temperature to ensure complete evaporation.
- Suction superheat: Maintained at 35 K to prevent wet compression
- Steam pressure and compressor speed: Varied based on test point requirements.

The economizer could be activated or deactivated, and the portion of the working medium entering the compressor's super-feed port was regulated by an expansion valve. The adopted control strategy ensured full evaporation by maintaining a $10\,^{\circ}\text{C}$ temperature difference but may not be feasible in practical applications where waste heat temperature fluctuates.

2.2.3. Instrumentation

The performance data obtained for the heat pump is indicative in nature, with a best effort made to ensure validity. For example, condenser duty was cross-verified using two independent methods: the measured pentane mass flow and the steam mass flow. Good agreement was observed between these calculations, demonstrating reliability for the purposes of digital twin development. The key instruments used in the experimental setup (heat pump and test rig) are detailed below and can be visualized in Fig. 1:

Heat pump system:

- Pentane mass flow meter located in the main loop between the economizer and the main expansion valve where the pentane is in liquid state. Specifications: Endress & Hauser Proline Promass F 300 Coriolis flowmeter DN80
- Pentane mass flow meter location in the economizer feed line, between the internal heat exchanger and the economizer expansion valve. Specifications: Endress & Hauser Proline Promass F 300 Coriolis flowmeter DN15
- Pentane mass flow over the condenser is the sum of the two mass flow meters (in steady state)



Fig. 2. TNO Carnot Laboratory including the pentane HP in the front and the test rig in the back.

- Pressure sensor: Danfoss AKS 33
- Temperature sensor: Pt100 resistance temperature detectors (not further specified by Mayekawa)

Test rig:

- Steam volume flow located after the expansion valve such that the steam is dry/superheated. Specifications: Krohne vortex flowmeter OPTISWIRL 4200 C DN150
- Pressure sensors: Endress & Hauser Cerabar M PMC51
- Temperature sensors: Endress & Hauser RTD Thermometer TR10 with Pt100 element installed in a thermowell
- Waste heat volume flow: Krohne ultrasonic flowmeter OPTISONIC 3400 F DN125

As the TNO Carnot Laboratory operates as a field laboratory for industrial-scale prototypes, it emphasizes replicating real-world operational conditions over rigorous laboratory-grade calibration. Consequently, calibration of all instruments was not prioritized, considering the cost and effort relative to the goals of this study. Uncertainty in indirect measurements such as heat output and COP is acknowledged but was not rigorously quantified. The experimental data is intended to provide a solid foundation for the validation and development of the digital twin rather than for certifying the precise performance of the heat pump prototype.

2.2.4. Experimental testing of the heat pump

The intended nature of the TNO FUSE project was to demonstrate a steam producing heat pump at an industrially relevant size (1 MWth heat duty); troubleshoot the prototype HP and finetune the control parameters before going to an industrial site. Therefore, the primary goal of the experimental campaign was to determine the HP's operational stability under varying external conditions and loads. The compressor speed served as an indicator of HP load. Each combination of source, sink, and speed defined an HP operating point, maintained stable for about 30 min. For most operating points, the economizer was disabled, as its impact on performance was not the primary focus of this study. A total of 55 steady-state operating points were tested, with a subset presented in Table 1 including comparison of the actual COP (1) to its theoretical limit COP_{ext} following (3) via fraction COP_{ext}^* defined

in (5). These conditions include variable source temperature, pentane evaporation pressure, steam pressure, and compressor speed. The rest of input parameters of the system are maintained constant: water feed flow rate (68 m³/h per evaporator), evaporator pentane pressure (pentane saturation 10 K below source temperature), and compressor suction superheat (35 K).

While a simplified energy balance comparison is often used to validate heat pump systems, it is not applicable here due to the presence of significant and unquantified heat losses from the ventilated enclosure and known oil cooling requirements. The heat pump setup prioritizes operational safety and prototype development under industrially relevant conditions, where precise energy balance validation was not a primary goal.

2.3. Digital-twin development

This section outlines our methodology for developing a digital twin of the HP using measurement data from the experimental setup discussed in the previous section. The workflow for creating the digital twin of the HP investigated in this study is schematically shown in Fig. 3. As previously detailed, 55 measurements were conducted across both operating stages, with and without the economizer, by varying the water inlet temperature, volumetric flow rate on the waste-heat source side, compressor rotational speed, and steam pressure. These parameters varied within the ranges of 65 °C to 97 °C for water inlet temperature, 68 m³/h to 70 m³/h for volumetric flow rate, 1500 RPM to 3000 RPM for compressor speed, and 1.5 bar to 3.5 bar for steam pressure, respectively. A full-order model of the HP based on these measurements was developed. The data from the full-order model were categorized into two groups: independent parameters (water temperature, volumetric flow rate, compressor rotational speed, and steam pressure) and objective functions (mass flow rate, temperature, pressure at the components' boundaries, and compressor electric power consumption). GPR was applied to the reduced data set, enabling the prediction of the objective functions, the calculation of performance metrics such as COP and heating duty. This framework outlines the digital twinning methodology for the FUSE HP.

Table 1
Subset of experimental results of TNO HP. Design reference condition in **bold**. Tests 1–10: economizer disabled; test 11 is test 10 with economizer enabled. Fraction of Carnot COP concerns COP_{ext}^* following (5).

Test	Source temperature	Sink temperature	Compressor speed	Heating duty	COP	Fraction of Carnot COP
	[°C]	[°C]	[RPM]	[kW]	[-]	[%]
1	91	142	1500	435	2.3	28
2	63	144	2700	420	1.3	24
3	97	140	2700	905	2.7	28
4	91	140	2700	823	2.4	29
5	91	135	2700	840	2.7	29
6	91	130	2700	836	2.9	28
7	96	135	2700	900	2.8	27
8	64	105	2700	584	3.2	34
9	65	123	2700	522	2.1	31
10	77	140	3000	642	1.7	26
11*	77	140	3000	788	1.9	29

2.3.1. Gaussian process regression

The objective is to create a model of a physical process by regressing a function y = f(x) to data

$$\vec{x} = \{x_1, x_2, \dots, x_M\}, \qquad \vec{y} = \{y_1, y_2, \dots, y_M\},$$
 (6)

on dependent (y) versus independent (x) process variables. Traditionally, this is done by fitting a polynomial expansion using the least-squares method. However, a significant limitation of this approach is its dependence on a predefined and possibly suboptimal functional form.

Gaussian Process Regression (GPR) offers a non-parametric alternative by fitting the mean of a distribution of functions to data (6). This involves two steps. First, the definition of a set of candidate functions ("prior distribution") and, second, isolation of the subset of functions that run through data (6) (posterior distribution). The essence of GPR is elaborated below and based on [30,31].

The prior distribution consists of a Gaussian distribution of possible function values $f(X_i)$ on a grid $\vec{X} = \{X_1, \dots, X_D\} = \vec{x} \cup \vec{x}_*$ of D positions X_i comprising of data points (6) and $N = D - M \geq 1$ positions $\vec{x}_* = \{x_1^*, \dots, x_N^*\}$ on which to determine the GPR model. Each candidate function $\vec{f} = \{f(X_1), \dots, f(X_D)\}$ is a realization of the D-dimensional multi-variate normal (MVN) distribution $\mathcal{N}_D(\vec{f}, \Sigma_D)$ around mean \vec{f} . Covariance matrix $\Sigma_D = \Sigma_D^\dagger$ correlates the function values $f(X_{i,j})$ via the independent variables $X_{i,j}$ through

$$\Sigma_{ij} = K(X_i, X_j), \qquad K(X_i, X_j) = \sigma_K^2 \exp\left[-\frac{1}{2} \left(\frac{X_i - X_j}{L}\right)^2\right], \tag{7}$$

with $K(X_i,X_j)$ the kernel († indicates transpose). The kernel plays a critical role in determining the smoothness of functions $f(X_i)$ such that they are suitable for interpolation purposes and are here defined by the Radial Basis Function (RBF) kernel, specified by the hyperparameters σ_K and L. Fig. 4(a) shows sample candidate functions (colored curves) of the prior distribution on grid $\vec{X}=\vec{x}\cup\vec{x}_*$ comprising of M=10 and N=500 equidistantly-placed data (x_i) and interpolation (x_i^*) points, respectively, using zero mean $\vec{f}=\vec{0}$ (gray line) and kernel (7) for $\sigma_K=1$ and L=0.15.

The posterior distribution consists of the subset of functions in the prior distribution that runs through the data. Fig. 4(a) includes artificial data \vec{y} (black dots) generated on \vec{x} by the function $f(x) = \sin 2\pi x$ and shows that most candidate functions violate this requirement and must be eliminated from the prior distribution. This can be achieved by Bayesian inference, yielding the posterior distribution $\vec{f}_* = \{f(x_1^*), \dots, f(x_N^*)\} \in \mathcal{N}_N(\vec{f}_*, \Pi)$ on \vec{x}_* , with

$$\vec{f}_* = \Sigma_*^{\dagger} \Sigma^{-1} \vec{y}, \qquad \Pi = \Sigma_{**} - \Sigma_*^{\dagger} \Sigma^{-1} \Sigma_*, \tag{8}$$

as mean and covariance, respectively, and $\Sigma_{i,j} = K(x_i,x_j)$, $\Sigma_{*,i,j} = K(x_i,x_j^*)$ and $\Sigma_{**,i,j} = K(x_i^*,x_j^*)$ covariances between/within subgrids \vec{x} and \vec{x}_* . Fig. 4(b) shows mean \bar{f}_* and two realizations $f_{1,2}$ on subgrid \vec{x}_* for the beforementioned artificial data \vec{y} including the uncertainty

bound demarcated by standard deviation $\sigma(x_i^*) = \Pi_{ii}^{1/2} \sim \mathcal{O}(0.02)$ (shaded region).

The mean of posterior distribution (8) defines the GPR process model, viz. $y(x) = \bar{f}_*(x)$, and its prediction quality is quantified by the Coefficient of Determination (COD) R^2 , i.e.,

$$R^{2} = 1 - \frac{\sum_{i=1}^{N} (y_{o,i} - y_{p,i})^{2}}{\sum_{i=1}^{N} (y_{o,i} - \text{mean}(\vec{y}_{o}))^{2}},$$
(9)

with $y_{o,i}$ and $y_{p,i} = \bar{f}_*(x_i^*)$ the observed and predicted function values, respectively, on \vec{x}_* (R^2 closer to unity signifies better prediction) [32].

The above describes the basic approach behind GPR and generalizes to problems with multiple independent variables $y = f(x_1, x_2, ...)$ and data subject to noise. Moreover, the hyperparameters (σ_K, L) for kernel (7) have been chosen manually for the example in Fig. 4 yet optimal settings can be systematically obtained by hyperparameter optimization [30,31].

2.3.2. Process models

The digital twin of the HP will consist of process models for each relevant process variable, derived from datasets (6) using Gaussian Process Regression (GPR) as described in Section 2.3.1. The independent variables x include user-defined inputs such as the waste-water temperature T_{water} , the waste-water volumetric flow rate \dot{V}_{water} , compressor rotational speed ω_{comp} , and the boiling pressure of water P_{steam} in the condenser. The corresponding dependent variables y include measured outputs like compressor outlet pressure and temperature.

The aim of this study is to predict the HP's performance in terms of the indicators COP and $\dot{Q}_{heating}$ as introduced in Section 2.1 as well as monitor thermodynamic state variables at the boundaries of each HP component. To achieve the digital twin of the HP for estimating the system performance, we first need process models for the working-medium mass flow rate $\dot{m}_{comp,out}$, compressor electric power consumption $\dot{W}_{comp,electric}$, and compressor outlet temperature $T_{comp,out}$, and pressure, $P_{comp,out}$. The mass flow rate, power consumption, and outlet temperature vary with all independent parameters, while the outlet pressure depends only on the steam inlet pressure on the condenser's cold side. Fig. 5 depicts the GPR modeling of each component for estimating flow variables and parameters necessary for performance prediction.

The GPR process models are derived from datasets obtained from 55 steady-state operating points (Section 2.2). As schemed in Fig. 5, the compressor data models are used for estimating the parameters ($P_{comp,out}$, $T_{comp,out}$, $m_{comp,out}$, and $\dot{W}_{comp,electric}$) required for the system performance calculations. Thermodynamic properties derived from the dependent variables, specifically the enthalpies $h_{comp,outlet}$ ($h_{condenser,hot,inlet}$) and $h_{condenser,hot,outlet}$ in Eq. (2), are evaluated using the open-source CoolProp libraries [33], assuming the conditions given in Section 2.1. The condenser data model determines the flow variables under the assumption that the outlet conditions are those of a saturated liquid. The data models of the other components are developed to

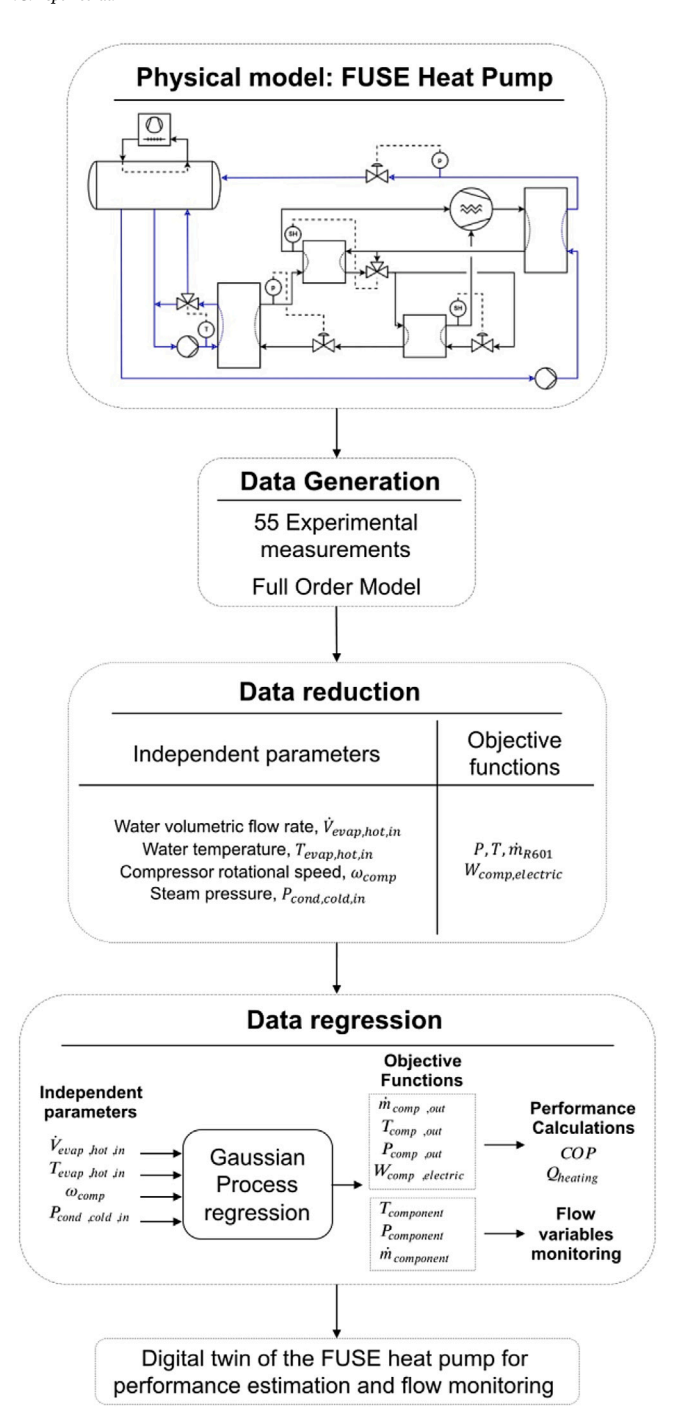


Fig. 3. Schematic illustration of the digital twining methodology for the FUSE HP.

predict flow variables at the components' boundaries, such as the temperature at the superheater's cold side outlet.

It is worth noting that the pressure drops along the internal heat exchanger and economizer hot sides are negligible. Therefore, we assumed that the inlet pressure at the hot side is equal to the outlet pressure in the modeling of these components. The internal heat exchanger cold inlet conditions are the same as those at the evaporator outlet. Similarly, the economizer cold outlet temperature is found by the heat balance equation written between the hot and cold sides of the component. An isenthalpic expansion process determines the flow conditions at the evaporator's inlet through the expansion valve. Depending on the operating mode (stage with or without economizer),

the isenthalpic expansion calculations are conducted between the distributor (expansion valve) data model and either the superheater or economizer data models to compute the evaporator inlet quality (see Fig. 5).

Some of the objective functions' data models were created using separate data sets for operating stage with economizer (39 observations) and without economizer (16 observations) in order to enhance prediction accuracy. The models derived for operating stages with and without economizer are employed to predict objective functions based on the user-specified operation type. In the validation section of the digital twin model, we will discuss the prediction accuracy of the data models by presenting the R^2 (COD) values for the objective functions and showing their parity plots.

Monitoring the flow variables, along with calculating and analyzing system performance as a function of independent parameters, constitutes the digital twin of the studied HP. The system performance parameters – heating duty and compressor electric power consumption – provided by the digital twin for a given set of independent parameters are used as inputs for the economic and environmental evaluation of the HP. In the next section, we will provide the details of this evaluation.

2.4. Economic and environmental assessment of the heat pump

Relevant for determining the practical usefulness of the HP is an assessment of its economic and environmental performance. This assessment will be done in terms of energy savings ($E_{savings}$), CO₂ reductions (CO_{2,savings}), and payback time (PBT) for various operational scenarios, comparing to a steam boiler using propane as fuel and based on a case study in the Netherlands.

The required parameters for this analysis include the unit price of electricity consumed in industry ($\lambda_{electricity,NL}$), the primary energy conversion factor (indicating electricity production efficiency) (ϕ_{energy}), annual operating hours t, annual inflation and interest rates, the lower heating value (LHV) of propane, propane boiler efficiency (η_{boiler}), total costs of the heat pump (HP) (Λ_{HP})—which encompass installation costs (given in euros per kWh) and integration costs (assumed to be half of the installation cost)—propane price ($\lambda_{propane}$), the conversion factor for CO₂ emissions per kilogram of propane combustion, CO₂ taxes on propane, and CO2 taxes on emissions. These parameters are shown in Table 2 with the references, where in several cases we must resort to assumptions for their values. Additionally, the heating duty, compressor electric power consumption $\dot{W}_{comp,electric},$ and mechanical efficiency of the electric motor $\eta_{mechanical}$, which are provided by the digital twin for specific independent parameter features, are also necessary for this analysis.

Several resources were referenced for the assumed values presented in Table 2. For the boiler efficiency, a high-efficiency heating system is considered one in which the boiler can convert chemical energy into thermal output with a minimum efficiency of 90%, as specified by the U.S. Department of Energy [34]. The electricity in the Netherlands is generated from various sources, including renewable energy, natural gas, coal, and oil. The energy conversion factor, reflecting the efficiency of electricity production, can vary depending on the type of installation and the energy source used. We assume that mechanical losses during the conversion process, attributed to generator efficiency [35], result in an overall conversion factor of 90%. The assumed installation and integration costs for industrial heat pumps was set at 700 €/kWth. These values are consistent with those reported in the literature [36, 37]. The integration cost is highly dependent on the type of industrial process and the specific application of the project (e.g., Brownfield or Greenfield). For the purposes of this study, it was guessed to be half the cost of the installation.

One of the main outputs of this work is the $E_{\it savings}$, achieved by using a HP instead of a propane boiler. These savings are calculated via

$$E_{savings} = \dot{Q}_{propane} - E_{electric,compressor}$$
 [MWh/year] (10)

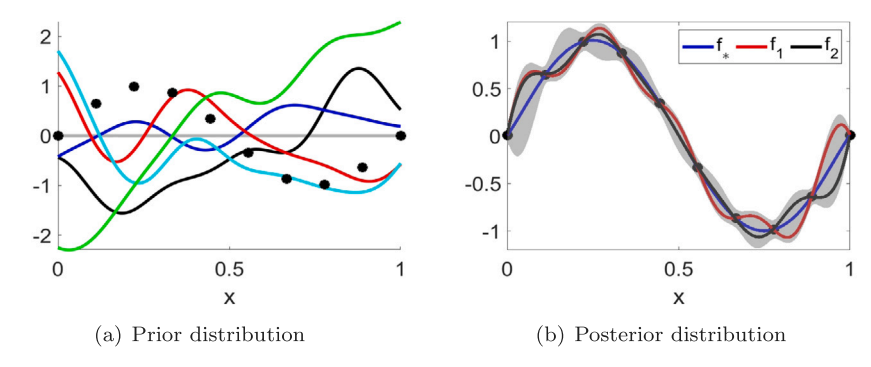


Fig. 4. GPR model $y = \bar{f}_*(x)$ defined by mean \bar{f}_* of posterior (right) determined by restricting prior (left) to training data \vec{y} (black dots). Curves other than \bar{f}_* : realizations of prior/posterior distributions; shaded region: uncertainty bound $\bar{f}_*(x) \pm \sigma(x)$ (amplitude exaggerated for visibility).

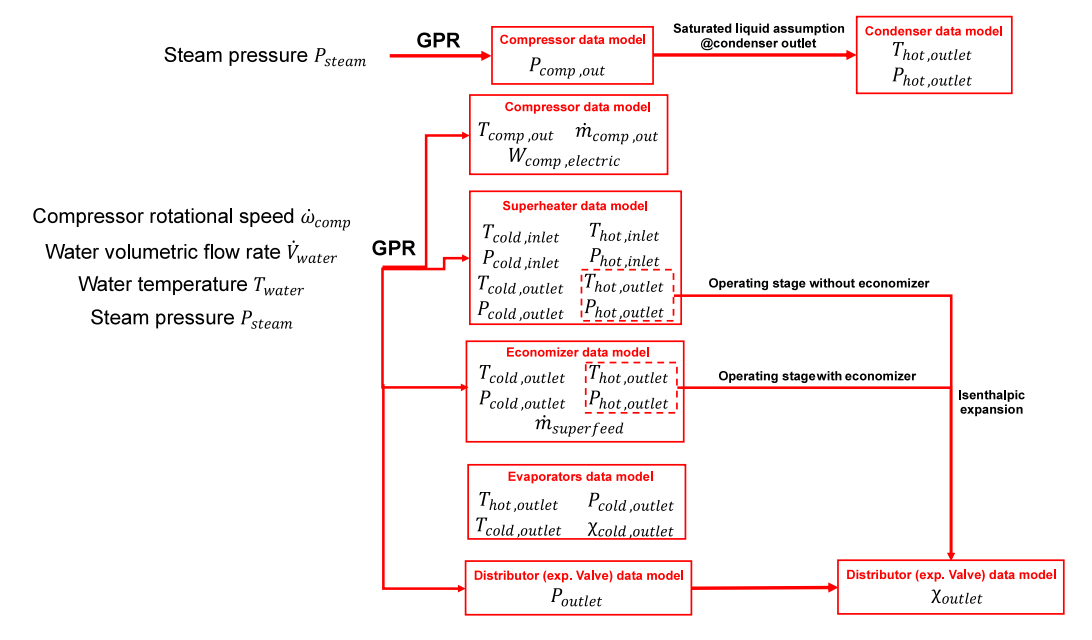


Fig. 5. Process models of each component and objective function estimated via GPR for given independent parameters.

 Table 2

 Parameters needed for the economic and environmental assessment.

Parameter	Explanation	Value	References
$\lambda_{\text{CO}_2 taxes, NL}$	CO ₂ taxes in the Netherlands	74.17 €/tonCO ₂	[38]
$\lambda_{electricity.NL}$	Electricity price in the Netherlands	0.13 €/kWh	[39]
$\lambda_{propane}$	Propane price Euro/kWh	0.11 €/kWh	[40]
λ_{HP}	HP installation and integration costs per kWth	700 €/kWh & 350 €/kWh	Assumption
$\phi_{{ m CO}_{2,propane}}$	Conversion factor of CO ₂ production per burnt propane	2.933	[41]
$\eta_{mechanical}$	Electric motor efficiency	Data-driven model	_
ϕ_{energv}	Energy conversion factor regarding electric production efficiency	0.9	Assumption
t	Operating hours per year	3600 hr/year	Assumption
η_{boiler}	Boiler efficiency	0.9	Assumption

where the annual heating by the boiler, $\dot{Q}_{propane}$, is computed via

$$\dot{Q}_{propane} = \frac{\dot{Q}_{system} \cdot t}{1000 \cdot \eta_{boiler}}$$
 [MWh/year] (11)

with \dot{Q}_{system} the required heating duty by the industrial process. The annual electricity consumption by the HP compressor to provide \dot{Q}_{system} instead of the propane boiler is calculated from

$$E_{electric,compressor} = \frac{\frac{W_{comp,electric} \cdot t}{1000 \cdot \eta_{mechanical}}}{\phi_{energy}}$$
 [MWh/year] (12)

where in both (11) and (12) we assume that the system operates 18 h per day and 200 days per year for calculating time t ([hr/year]).

Quantifying energy savings is crucial to assess how much energy can be conserved by using the heat pump (HP) in place of the propane boiler system. From an environmental standpoint, reducing emissions (one of the major concerns with fossil-fueled systems) is just as important as achieving energy savings. Therefore, another significant outcome of this work is the reduction in CO_2 emissions achieved by using an HP instead of a propane boiler, denoted as $\mathrm{CO}_{2,savings}$, which is calculated by

$${\rm CO}_{2,savings} = {\rm CO}_{2,produced-propane} - {\rm CO}_{2,produced-electricity} \hspace{1cm} [ton/year]$$

(13)

$$PBT = \frac{\Lambda_{HP}}{\Lambda_{propane} + \Lambda_{\text{CO}_2 - taxes, propane} - E_{electric, compressor} \cdot \lambda_{electricity, NL} - \Lambda_{\text{CO}_2 - taxes, electricity}}, \qquad [year]$$
(17)

Box I.

where the emissions produced by the propane combustion in the boiler follow from

$$CO_{2,produced-propane} = \dot{m}_{propane} \cdot \phi_{CO_{2,propane}},$$
 [ton/year] (14)

using

$$\dot{m}_{propane} = \frac{t}{1000} \cdot 3600 \cdot \frac{\dot{Q}_{system}}{LHV \cdot \eta_{Boiler}},$$
 [ton/year] (15)

to compute the propane mass flow rate $\dot{m}_{propane}$.

The emissions $CO_{2,produced-electricity}$ produced by the HP result from the electricity consumption by its compressor and can be evaluated as follows. Renewable sources provide a large part of the annual electricity production (\approx 44%) in the Netherlands [42] in 2022. The remaining portion is generated from fossil fuels, including natural gas (39.3% of overall production with 0.198 kg of CO_2 emissions per kWh [43]), oil (1.3% of overall production with 0.238 kg of CO_2 emissions per kWh [41]), and coal (14.3% of overall production with 0.4 kg of CO_2 emissions per kWh [43]). This yields

$$\begin{aligned} \text{CO}_{2,produced-electricity} &= E_{electric,compressor} \cdot (14.3\% \cdot 0.4\\ &+ 1.3\% \cdot 0.238 + 39.3\% \cdot 0.198), \end{aligned} \text{[ton/year]}$$

(16)

as a portion of the annual ${\rm CO}_2$ emissions caused by the total electricity production that results from the power consumption by the HP compressor.

Implementing the HP in place of the propane boiler for industrial applications in the Netherlands can lead to significant energy savings and reductions in ${\rm CO_2}$ emissions. These savings allow the HP system to recover its costs within a few years, depending on the specific industrial conditions, such as heating duty and steam pressure. As a result, another key outcome of this analysis is the simple payback time (*PBT*), which is defined as (see the Eq. (17) in Box I), which indicates the time it takes for the HP investment to be amortized without considering inflation or interest rates. Here, the total cost of the HP, Λ_{HP} , follows from the heating duty of the HP and the unit total cost of the HP, λ_{HP} , via

$$\Lambda_{HP} = \frac{\dot{Q}_{heating} \cdot \lambda_{HP}}{1000} \qquad [k \in]. \tag{18}$$

The annual price for propane consumption if heating by the boiler instead of the HP is given by

$$\Lambda_{propane} = \lambda_{propane} \cdot \dot{Q}_{propane} \qquad [k \in]$$
 (19)

and the corresponding CO_2 taxes on the propane consumption are determined from

$$\Lambda_{\text{CO}_2-taxes,propane} = \frac{\text{CO}_{2,produced-propane} \cdot \lambda_{\text{CO}_2 taxes,NL}}{1000} \quad [k \in] \quad (20)$$

where $\lambda_{\text{CO}_2 taxes, NL}$ represents the applied CO_2 taxes in the Netherlands. Additionally, CO_2 emissions resulting from electricity production need to be considered when calculating payback time and are determined using:

$$\Lambda_{\text{CO}_2-taxes,electricity} = \frac{\text{CO}_{2,produced-electricity} \cdot \lambda_{\text{CO}_2 taxes,NL}}{1000} \qquad [k \in] \quad (21)$$

The performance outputs from the digital twin, such as heating duty and compressor electric power consumption, are used as inputs to calculate $E_{savings}$, $\mathrm{CO}_{2,savings}$, and PBT based on the equations provided above. The results will be analyzed in the following section using economic assessment maps.

3. Results

This section summarizes the steady-state HP performance throughout 55 measurement points obtained with varying water properties on the waste-heat source, compressor rotational speed, and steam pressure. It outlines the validation of the digital twin model established in this work. In addition, operating maps of the HP obtained by the digital twin approach in terms of COP and heating duty, and an economic and environmental assessment of employing the system in an industrial application in the Netherlands instead of using a fossil-fueled boiler are presented.

3.1. Experimental analysis

This sub-section of the report discusses the experimental results from running the industrial heat pump with the test rig at the TNO Carnot Laboratory. In Fig. 6, the heating duty and COP are plotted as functions of temperature lift. The vertical scattering of the heating duty at low-temperature lifts results from the varying sink and source temperature combinations. Notably, cases with very low source temperatures exhibit low heat sink duties despite moderate temperature lifts. As anticipated, the COP demonstrates a linearly decreasing relationship with temperature lift.

Overall, there is good agreement between the duties measured on the pentane and water sides. A source temperature of approximately 90 °C and a sink temperature of around 140 °C align well with the HP design and use pentane as the working medium. Butane may be better suited as a working medium for lower source temperatures due to its higher density at the compressor suction port, resulting in a higher heating duty. For extreme temperature lifts, a two-stage cascade system with suitable working medium could be considered as an alternative.

The resulting fraction of the Carnot COP, defined as COP_{ext}^* following (5), for each test is shown in Table 1 and ranges from 24% to 34%. This is significantly lower than the 50% typically applied to determine practical efficiency. Possible reasons for this include:

- Tailored Compressor Rotors: The current rotors yield reduced volumetric efficiency, which measures the volume transported from suction to discharge compared to the swept volume of the compressor. This is a consequence of being the first time such rotors were used for high-temperature conditions. Additional tests are planned with a redesigned rotor set optimized based on the presented test data.
- Low Intrinsic Volume Ratio of the Compressor: Significant under-compression occurs, especially at higher temperature lifts, leading to lost work and reduced efficiency. The upcoming tests will include an improved compressor volume ratio to better match the process conditions.
- 3. Large Approach Temperatures in Heat Exchangers: On the source side, suboptimal flow distribution of pentane in the evaporator section may cause inefficient use of the available heat transfer area. Fine-tuning the HP control system is expected to enhance internal heat reuse and reduce the need for evaporator superheat. A large portion of the required superheat at the compressor inlet will be provided by the internal heat exchanger. On the sink side, evidence suggests non-condensable gases are affecting the vapor–liquid equilibrium of the pentane, as approach temperatures near 10 K have been measured. This is

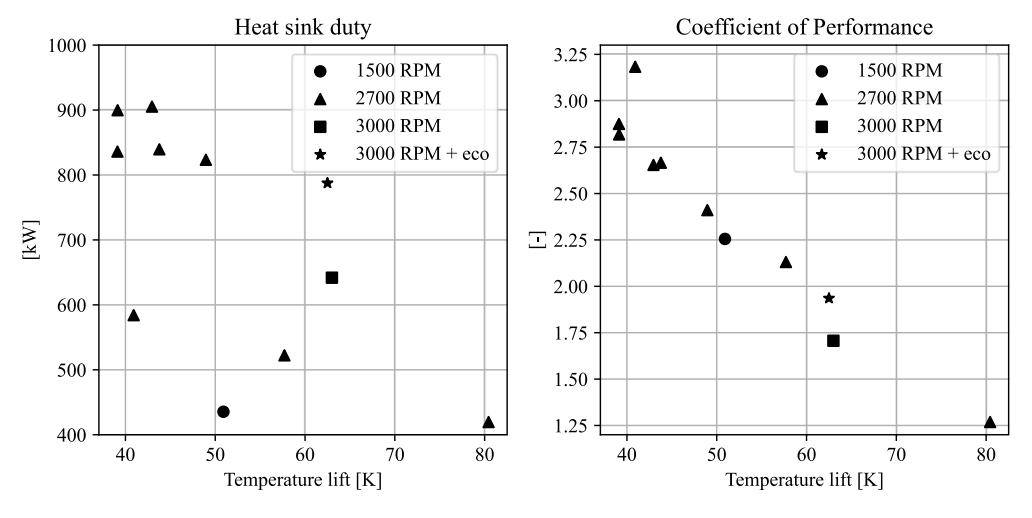


Fig. 6. Performance (heating duty on the left and COP on the right) of the industrial HP tested as a function of the temperature lift $(\Delta T_{lift} = T_{sink} - T_{source})$.

excessively high for a well-designed heat exchanger with phase changes on both sides. These non-condensable gases result from piping modifications and extended vacuum periods during system downtime, making their removal challenging. While large approach temperatures do not necessarily impact the HP internal performance, they significantly reduce the fraction of the Carnot COP based on the external temperature lift, i.e., COP_{ext}^* following (5). For instance, at the design condition, the internal fraction of the Carnot COP, i.e., COP_{int}^* following (5), is 44%, compared to 29% for the external fraction COP_{ext}^* .

The experimental campaign of a high-temperature HP in a laboratory environment was a success. The HP manufactured by Mayekawa Europe was successfully integrated and tested at the TNO Carnot Laboratory. We have demonstrated an industrial HP for a full range of operating conditions both at the source and sink, and we have identified potential areas of improvement. Moreover, the screw compressor designed by Mayekawa Japan was capable of running at higher temperatures using pentane as a working medium.

3.2. Validation of the digital twin

Process models for the dependent variables shown in Fig. 5 were developed as the functions of independent variables (ω_{comp} , T_{water} , \dot{V}_{water} , P_{steam}) using Gaussian Process Regression (GPR) as described in Section 2.3.2. For achieving this, 80% of the experimental data was randomly selected for training (\vec{x} , \vec{y}) as per Eq. (6). The remaining 20% was used as test data \vec{y}_o on interpolation points \vec{x}_* (see Section 2.3.1) to evaluate the models' prediction accuracy. This was done using the COD R^2 following Eq. (9) and parity plots that compare the observed values $y_{o,i}$ with the predicted values $y_{p,i} = \vec{f}(X_i)$ on $\vec{x} \cup \vec{x}_*$.

Table 3 provides the COD (R^2) for the dependent variables, showing values very close to unity (i.e., $R^2>0.98$ in most of the cases), indicating a high overall prediction quality of the process models. The corresponding parity plots are shown in Figs. 7 and 8, further substantiating this finding by revealing that the pairs ($y_{p,i}, y_{o,i}$) are concentrated closely around the line $y_{p,i}=y_{o,i}$, indicating error-free prediction. However, while the compressor outlet pressure ($P_{comp,out}$) and mass flow rate ($m_{comp,out}$) were predicted very accurately, discrepancies of up to 10% occur between the predicted and observed compressor outlet temperature ($T_{comp,out}$), evaporator A cold side outlet temperature ($T_{evapA,cold,outlet}$), and power consumption ($W_{comp,electric}$) in the higher ranges. This is perfectly acceptable in typical practical applications, demonstrating that the process models enable reliable prediction of the dependent variables.

Table 3 COD R^2 indicating prediction quality for dependent process variables. (The COD values of the process models built based on two datasets are given separated in the operating stage without economizer (second) and operating stage with economizer (third) columns. The COD values of the models built using the entire 55 observations are shown in a single combined column.)

Dependent variables	Overall R^2 (W/O econ. and With econ.)			
	Stage w/o econ.	Stage with econ.		
$\dot{m}_{comp,out}$		0.99		
$T_{comp,out}$		0.98		
$P_{comp,out}$		0.99		
$\dot{W}_{comp,electric}$		0.98		
P _{distributor,outlet}		0.99		
$P_{economizer,cold,outlet}$	N/A		0.99	
$\dot{m}_{economizer, superfeed}$	N/A		0.99	
$T_{economizer,hot,outlet}$	N/A		0.95	
$T_{evapA,cold,outlet}$	0.83		0.96	
PevapA,cold,outlet		0.99		
$T_{evapA,hot,outlet}$		0.99		
$T_{evapB,cold,outlet}$		0.99		
$P_{evapB,cold,outlet}$		0.99		
$T_{evapB,hot,outlet}$		0.99		
T _{superheater,cold,outlet}		0.93		
$\Delta P_{superheater,cold}$		0.97		
$T_{superheater,hot,outlet}$	0.97		0.93	

One of the primary reasons for the discrepancy between the measured and predicted data for evaporator A's cold-side temperature (see Table 3) could be attributed to experimental uncertainties. Although evaporators A and B are identical, their heat transfer rates differ due to variations in the mass flow rates of the working medium. These differences result in the working medium exiting the heat exchangers at different outlet temperatures. Consequently, variations in outlet temperature data, along with non-linearities introduced by measurement uncertainties, hindered the accuracy of the chosen regression model. As a result, the GPR model struggles to accurately capture the nonlinearity in evaporator A's cold-side outlet temperature dataset across the 39 observations. Additionally, a few points can be noted concerning the predictions of the compressor discharge temperature $(T_{comp,out})$ and power consumption ($\dot{W}_{comp,electric}$). The variations were mainly caused by experimental uncertainties, particularly related to oil losses within the system.

A vital aspect of this study is that the digital twin reliably predicts flow variables at the boundaries of the components and also, more importantly, performance indicators, such as COP and $\dot{Q}_{heating}$ (see Section 2.1). Fig. 9 presents the parity plots for COP and $\dot{Q}_{heating}$, derived from Eqs. (1) and (2) using observed versus predicted dependent variables. Similar to Figs. 7 and 8, these plots show a tight clustering

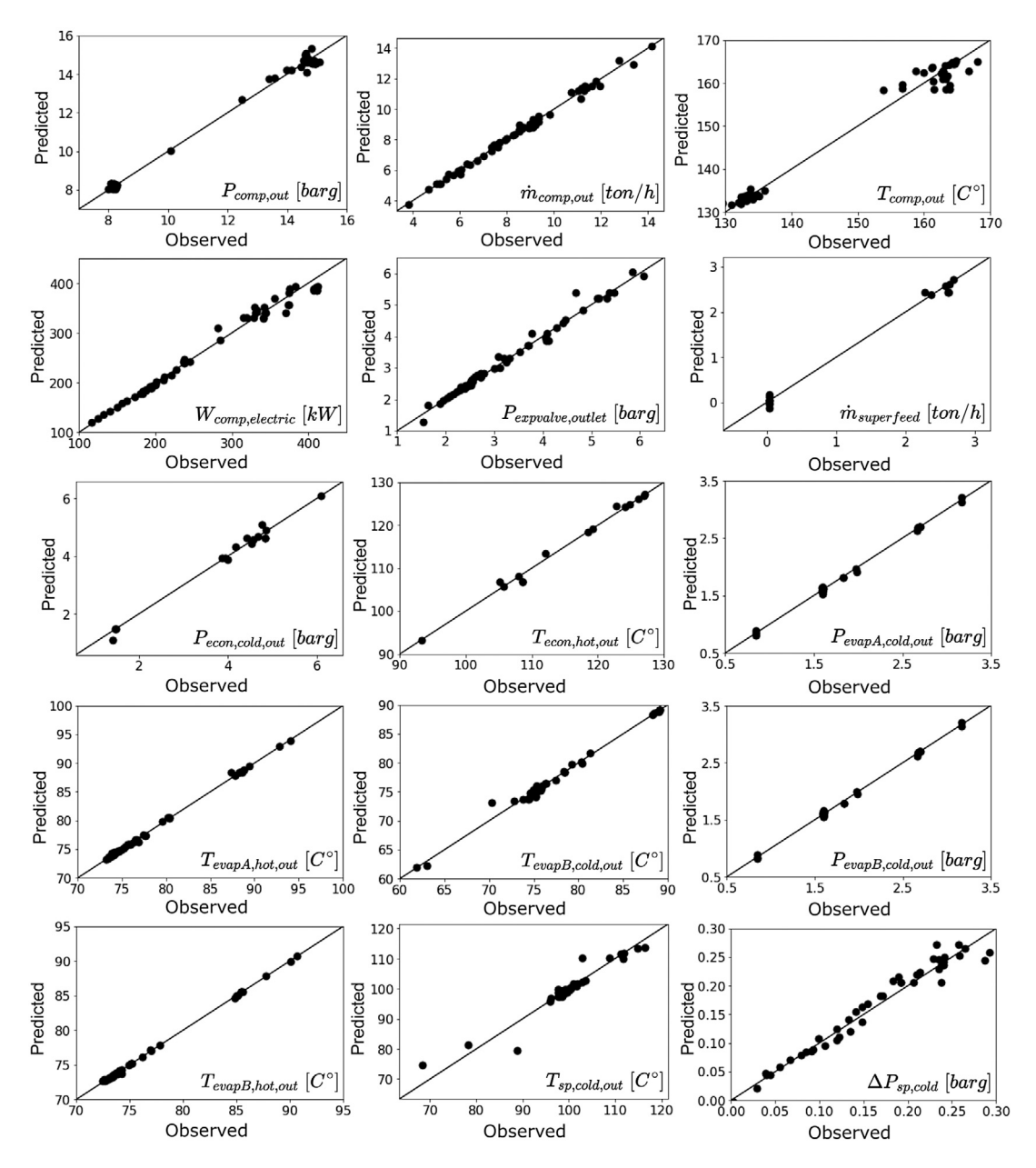


Fig. 7. Parity plots of the objective functions for which the entire dataset was used to generate the process models.

of points around the line $y_{p,i}=y_{o,i}$, indicating accurate predictions. The discrepancies for COP and $\dot{Q}_{heating}$ remain within 7%, suggesting that the more significant errors observed for $T_{comp,out}$ and $\dot{W}_{comp,electric}$ at higher ranges (Fig. 7) have only a minor impact. In conclusion, our digital twin accurately predicts HP performance within a 7% error margin.

3.3. Predicted performance of the heat pump

The digital twin of the HP enables us to determine system performance and changes in flow variables in response to variations in the independent parameters (ω_{comp} , T_{water} , \dot{V}_{water} , and P_{steam}). This section is devoted to analyzing the HP performance with variations in these independent variables. Fig. 10 shows the variation in HP performance, where the COP is color-coded, and the heating duty ($\dot{Q}_{healing}$) and compressor electric power consumption ($\dot{W}_{comp,electric}$) are depicted with solid and dashed lines, respectively.

An industrial process (using steam for its heat demand) is designed for a specific steam pressure and heating duty [44]. The HP performance is evaluated in this section by considering possible scenarios where the HP is employed to produce a certain steam pressure and a heating duty. Therefore, we have color-coded the COP for different steam pressures and plotted the heating duties with solid lines to demonstrate the design band of an industrial process (see Fig. 10).

As mentioned above, the water volumetric flow rate range is between $68~\text{m}^3/\text{h}$ and $70~\text{m}^3/\text{h}$. Our observations indicate that this narrow range does not significantly affect the system performance trend across varying independent parameters. Therefore, the performance maps are displayed only for the water volumetric flow rate of $70~\text{m}^3/\text{h}$.

It is important to note that the structure of the data models depends on the amount and range of data used for training and varies based on the type of operation, whether it is operating stage with or without economizer. Specifically, the valid compressor speed range for predicting operating stage without economizer performance with the digital twin is between 1500 and 3000 RPM, while it narrows to between 2700 and 3000 RPM for operating stage with economizer.

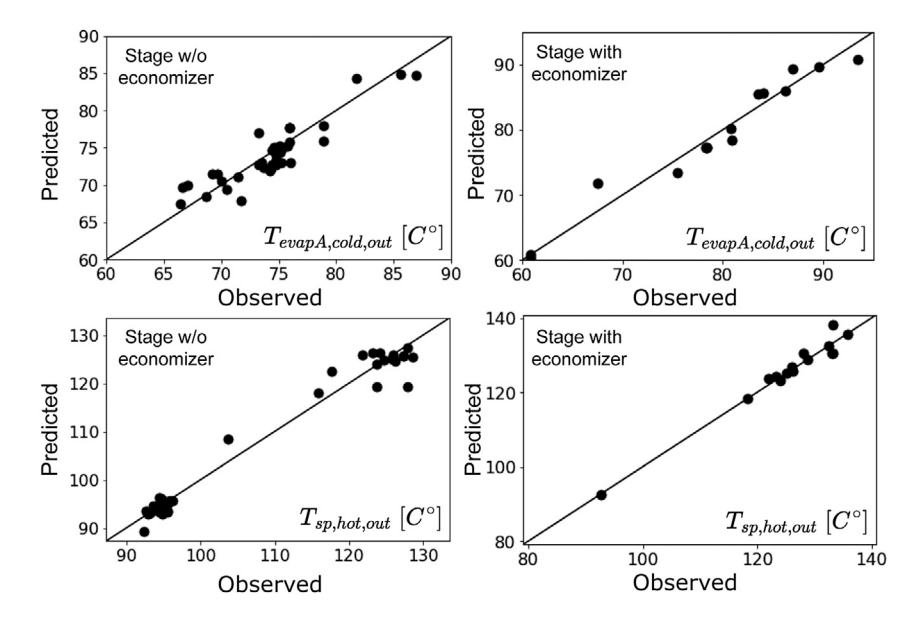


Fig. 8. Parity plots of the objective functions for which separate datasets were used based on the operating mode to generate the process models.

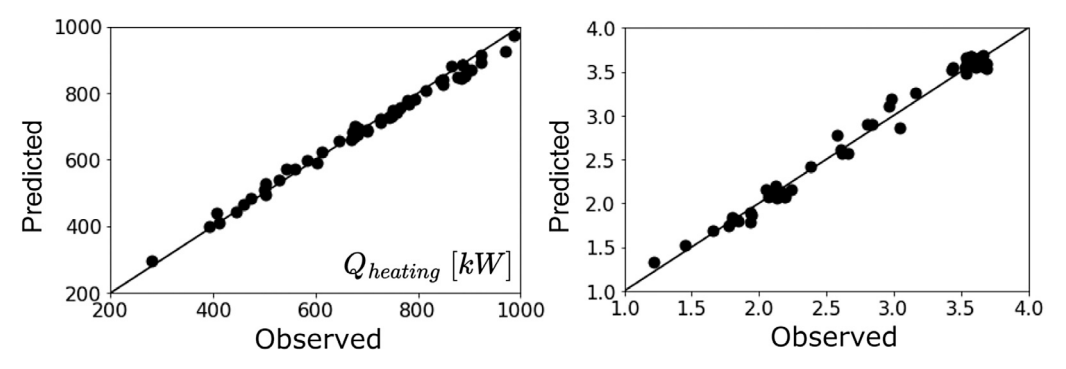


Fig. 9. Parity plots displaying prediction quality for performance indicators.

Another limitation regarding operating stage with economizer pertains to the steam pressure. All experimental measurements with economizer operation were carried out at a steam pressure of 3.5 bar absolute. Although these limit our ability to observe system performance over a broader range of independent parameters, particularly for compressor speed and steam pressure, the performance maps within the valid boundaries, as shown in Fig. 10, provide valuable insights into the system performance.

The white gaps in the performance maps indicate areas where the digital twin failed to produce physical solutions. Just as the data model's valid range restricted our ability to evaluate HP performance, the black-box model created in this study is only valid within the boundaries of physical solutions, as shown with colored zones in Fig. 10.

As anticipated, a higher water (source) inlet temperature and a reduction in steam pressure significantly improve the COP for both operating stages with and without economizer. The increase in source temperature and the reduction of steam temperature both result in a smaller temperature lift that the HP must overcome, reducing the required compressor power. The impact of steam pressure is less effective than that of water inlet temperature, which is the key parameter for calculating the heating duty of the system. Water temperature and compressor rotational speed also positively influence heating duty, although the effect of compressor speed is less strong than that of water temperature. Fig. 10 demonstrates that in operating stage without economizer, the maximum heating duty, approximately 1050 kW, can be obtained for all investigated boiler pressure values but with different COP values.

In the maps of operating stage without economizer, up to approximately 2600 RPM of compressor speed, compressor power consumption follows a curve, indicating that the required work decreases with increasing water temperature. Beyond 2600 RPM, it becomes insensitive to further changes in the water inlet temperature. This leads to achieving the optimum COP at around this rotational speed; this is the designed speed of the HP under investigation for producing 2.4 bar, 3.2 bar, or 3.5 bar steam pressure and providing around 1 MW heating duty to an industrial setting. The change in compressor power consumption with water inlet temperature diminishes for compressor speeds above approximately 2700 RPM, as observed across all steam pressures. This optimal rotational speed of the compressor was found to achieve a higher COP compared to other types of industrial high-temperature heat pumps operating with R601, under similar evaporation and condensation pressures [45]. According to the data provided for the compared heat pump in the reference, the COP was calculated to be 3.27. However, the analysis presented in this paper demonstrates that the COP can be further enhanced, exceeding 3.5, by optimizing the independent parameters for waste-heat water temperatures above 85 °C.

Due to the limited experimental data, the operating stage with economizer maps cover a narrower range of compressor speeds compared to the operating stage without economizer maps. Additionally, the digital twin was obtained for operating stage with economizer only at a steam pressure of 3.5 bar. The performance parameters – COP, heating duty, and compressor power consumption – show similar trends to those observed in operating stages without economizer. However, COP's

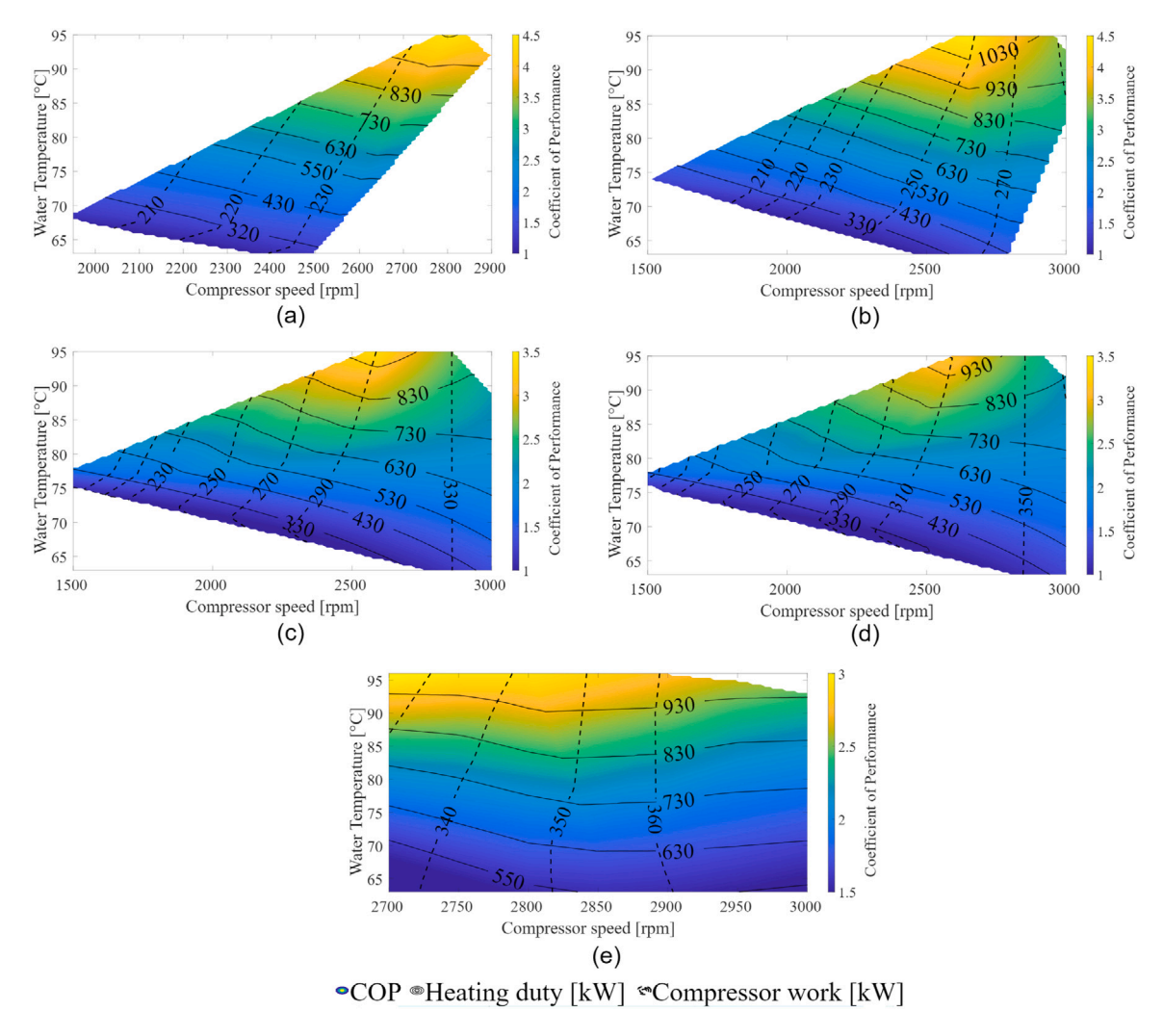


Fig. 10. Operating maps of the HP obtained by the digital twin (Maps for 1.9 bar (a), 2.4 bar (b), 3.2 bar (c), and 3.5 bar (d) steam pressures in the stage without economizer, a map for 3.5 bar (e) steam pressure in the stage with economizer).

dependence on compressor speed is notably smaller in operating stages with economizer. This is likely because we are examining a narrower range of the independent parameter. The highest efficiency zones were achieved at the highest heating duty with compressor speeds of 2700 RPM for a steam pressure of 3.5 bar in operating stage with economizer. In these zones, COP is computed to be approximately 3, which is higher than that of operating stage without economizer at the same steam pressure of 3.5 bar. This means that the economizer does provide a performance improvement to the HP as theoretically expected.

3.4. Economic and environmental assessment of the heat pump

This subsection focuses on the economic evaluation of the HP system when used within an industrial process in the Netherlands. As mentioned, any industrial application is designed to operate at a specific steam pressure and heating duty. Therefore, our analysis includes an economic investigation of the HP system for various possible operations designed at a certain steam pressure and heating duty. This is done like the performance analysis carried out in Section 3.3.

The details of the calculations for the economic assessment and quantifying environmental benefits of the system in terms of ${\rm CO}_2$ savings are given in Section 2.4. We integrated the required calculations for this assessment to the digital twin, and this enabled us to visualize energy savings as displayed in Fig. 11, in case of employing the HP instead of a regular propane-fueled boiler in industrial applications.

This figure also depicts the heating duty and ${\rm CO}_2$ savings with solid and dashed lines respectively.

In almost all HP operating scenarios, the system is expected to recover the investment within 3.8 to 4.2 years (single payback time, PBT) by recuperating waste heat, based on the economic inputs and assumptions from Table 2. Overall, employing the heat pump instead of the propane-fueled boiler results in energy savings. However, when the water temperature is below approximately 75 °C, depending on the compressor speed in some operating scenarios, no energy savings with the HP are achieved, and using the boiler appears slightly more advantageous due to the assumed energy conversion factor (ϕ_{energy}). The COP in the no-energy-savings region varies between 1.1 and 1.6. Nonetheless, even in this limited operating region, due to the taxes on CO_2 emissions associated with the propane-fueled boiler, the heat pump system could still pay for itself when used in place of the propane boiler.

The trends of energy savings and COP are quite similar to each other, as shown in Figs. 10 and 11. The highest energy savings, similar to the best COP performance, were achieved when the system was designed to operate at either 1.9 bar or 2.4 bar steam pressure and had maximum heating duty of approximately 1000 kW. This design can yield more 3000 MWh energy savings per year. If the application requires greater steam pressure, this results in the compressor consuming more power at a similar heating duty and reducing yearly energy savings.

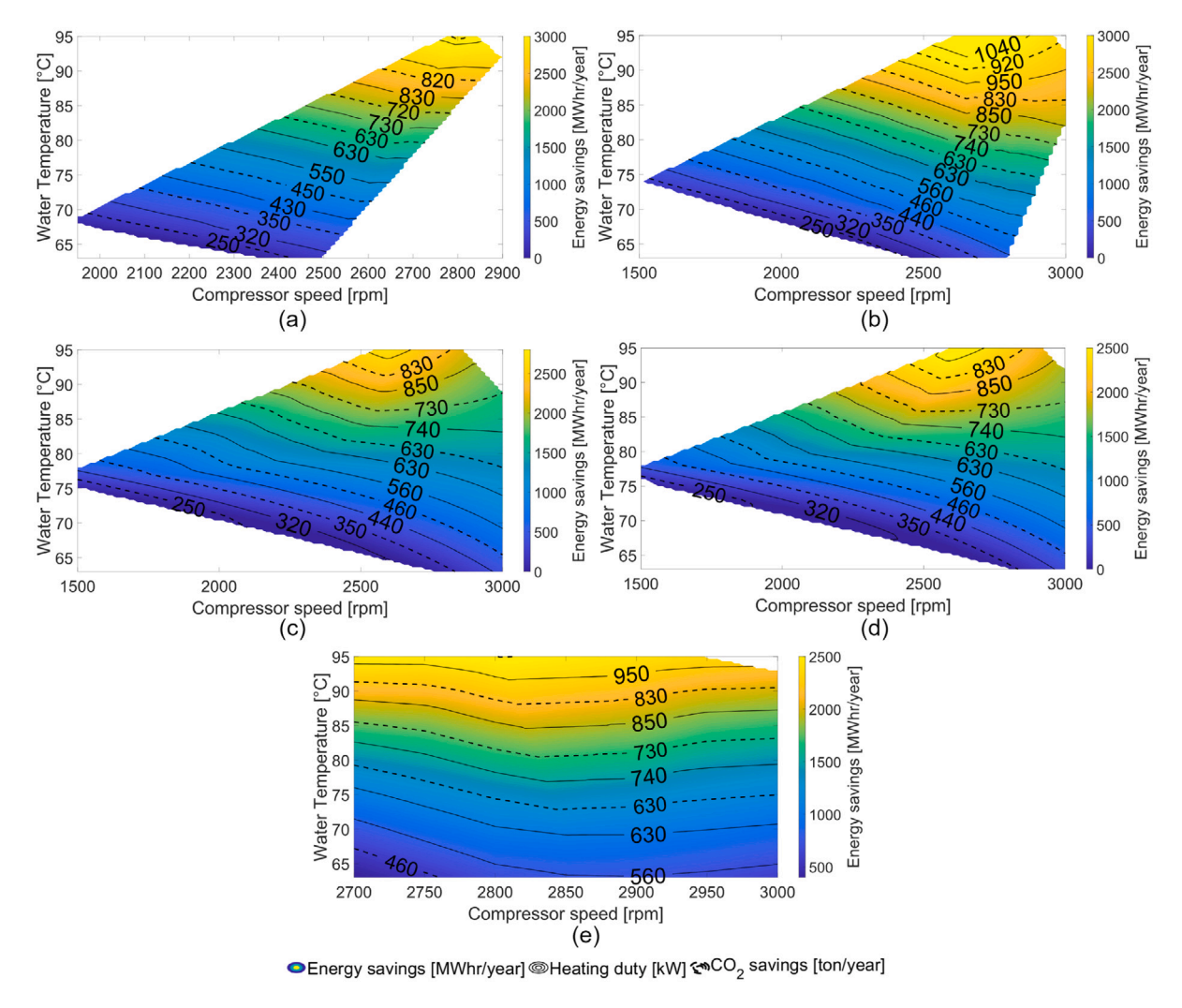


Fig. 11. Economic assessment maps of the HP obtained by the digital twin (Maps for 1.9 bar (a), 2.4 bar (b), 3.2 bar (c), and 3.5 bar (d) steam pressures in the stage without economizer, a map for 3.5 bar (e) steam pressure in the stage with economizer).

Although the adoption of the studied HP is challenged by limitations in water temperature on the waste-heat source and, to a lesser extent, compressor speed, for an industrial application replacing a fossil-fueled boiler, the system proves to be a more environmentally friendly solution by significantly reducing CO_2 emissions in all operational scenarios. The reduction rate naturally depends on the heating duty (Q_{system}) for which the industrial system is designed, following the same trend as the calculated heating duty shown in Fig. 11. The compressor power consumption also plays an important role in the CO_2 savings of the system since a significant portion of electricity production in the Netherlands is from sources where CO_2 is emitted. Therefore, it is possible to observe better savings in regions with less power consumption, such as the operating map drawn for 1.9 bar of steam pressure in Fig. 11.

The results of this study provided above reveal several opportunities for optimizing the industrial heat pump system, such as improving control strategies to enhance the COP and improve environmental impact under varying operational conditions such as compressor speed. These findings are particularly relevant to industries seeking to recover waste heat systems for process heating or district heating [46,47], where such optimizations can lead to significant energy savings and reduced carbon emissions. In real-world applications such as in process or petrochemical industries, this digital twin model can support predictive maintenance and operational decisions, ensuring the system operates at maximum efficiency over time. Future research could explore the

integration of machine learning algorithms for real-time optimization and expanding the model to include additional system variables for broader applications in energy-intensive industries.

4. Conclusions

This study introduces a novel method for developing a digital twin of an industrial heat pump (HP) utilizing n-Pentane as the working fluid. The system is designed to produce steam at 140 °C for industrial processes by heating an external water stream via the HP condenser (heating duty 1 MWth) through recovery of waste heat from a hot-water stream via the HP evaporator. Development of (digital twins of) HPs for waste-heat recovery and heat recuperation in industrial applications (especially operating with natural working media) are scarce to date and our study thereby represents a unique contribution to the literature.

The full-scale HP was successfully integrated and tested in a dedicated laboratory facility at TNO though the evaluation of 55 steady-state operating points. The HP achieved a Coefficient of Performance (COP) equal to 44% of the Carnot COP based on condenser/evaporator saturation temperatures, which can be further improved through compressor design changes and optimization of the control algorithm. A tailor-made digital twin as developed and calibrated in our study using the HP data from the laboratory facility enables this in a systematic and efficient way.

The digital twin consists of process models for each HP component developed using Gaussian Process Regression (GPR). It accurately

predicted key performance indicators like COP and heating duty from input variables such as compressor outlet pressure, temperature, mass flow rate, and electric power consumption, yielding prediction errors within 7%. The digital twin also reliably predicted relevant process variables for each HP component (e.g. outlet pressures and temperatures), with only minor errors that can be attributed to experimental uncertainties in the training data employed to develop the GPR process models.

An economic and environmental assessment demonstrated that the HP, when deployed in an industrial application in the Netherlands to replace a conventional propane boiler, could amortize its investment within 3.8 to 4.2 years. The system significantly reduces CO_2 emissions, ranging from 250 to 1000 tons per year, depending on operating conditions. Energy savings of over 3000 MWh annually are achievable when operating at steam pressures of 1.9 bar and 2.4 bar and a heating duty of 1 MWth during the steam generation. The HP overall achieves energy savings compared to a propane boiler (apart from a small operating region without an economizer). The temperature of the hot-water stream from which to recover waste heat is a critical parameter for energy savings: these savings become insignificant when this temperature falls below 75 °C.

The data-driven nature of the adopted modeling approach enables straightforward application for the digital twinning of other types of industrial HPs, provided sufficient experimental data are available. However, the most significant benefit lies in the potential to integrate HP digital twins thus developed into (digital twins of) broader industrial systems, enabling its utilization for enhancing system-wide efficiency and sustainability (i.e., beyond that of the HP itself). The potential impact of the digital twinning could be further expanded by exploring its use for real-time monitoring and predictive maintenance for the purpose of achieving long-term operational efficiency.

Declaration of competing interest

The authors declare that they have no known competing financial interests or personal relationships that could have appeared to influence the work reported in this paper.

Acknowledgments

The project is partially funded by the Topsector Energy subsidy of the Ministry of Economic Affairs and Climate Policy (EZK) of the Netherlands (project number MOOI42002). More details about the project can be found at https://projecten.topsectorenergie.nl/projecten/kickstart-market-industrial-heat-pumps-35646.

Data availability

The data that has been used is confidential.

References

- Final energy consumption in industry detailed statistics, 2024, https://ec.europa.eu/eurostat/statistics-explained/index.php?title=Final_energy_consumption_in_industry__detailed_statistics. (Accessed 12 March 2024).
- [2] Greenhouse gas emission statistics air emissions accounts, 2024 https://ec.europa.eu/eurostat/statistics-explained/index.php?title=Greenhouse_gas_emission_statistics_-air_emissions_accounts. (Accessed 12 March 2024).
- [3] R. de Boer, A. Marina, B. Zühlsdorf, C. Arpagaus, M. Bantle, V. Wilk, B. Elmegaard, J. Corberán, J. Benson, Strengthening industrial heat pump innovation: Decarbonizing industrial heat, 2020.
- [4] J. Tang, G. Gong, H. Su, F. Wu, C. Herman, Performance evaluation of a novel method of frost prevention and retardation for air source heat pumps using the orthogonal experiment design method, Appl. Energy 169 (2016) 696–708.
- [5] V.A. Arowoiya, R.C. Moehler, Y. Fang, Digital twin technology for thermal comfort and energy efficiency in buildings: A state-of-the-art and future directions, Energy Built Environ. 5 (5) (2024) 641–656.

- [6] M. Manfren, P.A. James, V. Aragon, L. Tronchin, Lean and interpretable digital twins for building energy monitoring—A case study with Smart Thermostatic Radiator Valves and Gas Absorption Heat Pumps, Energy AI 14 (2023) 100304.
- [7] M. Evens, A. Arteconi, Heat pump digital twin: An accurate neural network model for heat pump behaviour prediction, Appl. Energy 378 (2025) 124816.
- [8] C. Vering, S. Borges, D. Coakley, H. Krützfeldt, P. Mehrfeld, D. Müller, Digital twin design with on-line calibration for HVAC systems in buildings, in: Building Simulation 2021, Vol. 17, IBPSA, 2021, pp. 2938–2945.
- [9] A. Butean, J. Enriquez, A. Matei, A. Rovira, R. Barbero, S. Trevisan, A digital twin concept for optimizing the use of high-temperature heat pumps to reduce waste in industrial renewable energy systems, Procedia Comput. Sci. 237 (2024) 123–128.
- [10] J. Seifert, L. Haupt, L. Schinke, A. Perschk, T. Hackensellner, S. Wiemann, M. Knorr, Digital Twin for Heat Pump Systems: Description of a holistic approach consisting of numerical models and system platform, in: CLIMA 2022 Conference, 2022.
- [11] J.-H. Shin, Y.-H. Cho, Machine-learning-based coefficient of performance prediction model for heat pump systems, Appl. Sci. 12 (1) (2021) 362.
- [12] Y. Wang, W. Li, Z. Zhang, J. Shi, J. Chen, Performance evaluation and prediction for electric vehicle heat pump using machine learning method, Appl. Therm. Eng. 159 (2019) 113901.
- [13] X. Zhang, E. Wang, L. Liu, C. Qi, Machine learning-based performance prediction for ground source heat pump systems, Geothermics 105 (2022) 102509.
- [14] D. Zhou, Z. Zhu, A digital twin model for COP prediction in refrigeration system using combined machine learning method, in: 2022 IEEE Electrical Power and Energy Conference, EPEC, IEEE, 2022, pp. 412–417.
- [15] J.J. Aguilera, W. Meesenburg, W.B. Markussen, B. Zühlsdorf, B. Elmegaard, Real-time monitoring and optimization of a large-scale heat pump prone to fouling-towards a digital twin framework, Appl. Energy 365 (2024) 123274.
- [16] R. Lv, Z. Yuan, B. Lei, A high-fidelity digital twin predictive modeling of air-source heat pump using FCPM-SBLS algorithm, J. Build. Eng. 87 (2024) 109082.
- [17] J. Jiang, B. Hu, R. Wang, N. Deng, F. Cao, C.-C. Wang, A review and perspective on industry high-temperature heat pumps, Renew. Sustain. Energy Rev. 161 (2022) 112106.
- [18] A. Marina, S. Smeding, A. Wemmers, S. Spoelstra, P. Kremers, Design and experimental results of a two-stage steam producing industrial heat pump, in: 13th IEA Heat Pump conference, 2021.
- [19] C. Liu, W. Han, X. Xue, Experimental investigation of a high-temperature heat pump for industrial steam production, Appl. Energy 312 (2022) 118719.
- [20] L. Pan, H. Wang, Q. Chen, C. Chen, Theoretical and experimental study on several refrigerants of moderately high temperature heat pump, Appl. Therm. Eng. 31 (11–12) (2011) 1886–1893.
- [21] J. Navarro-Esbrí, A. Mota-Babiloni, Experimental analysis of a high temperature heat pump prototype with low global warming potential refrigerant R-1336mzz (Z) for heating production above 155°C, Int. J. Thermofluids 17 (2023) 100304.
- [22] M. Verdnik, R. Rieberer, Influence of operating parameters on the COP of an R600 high-temperature heat pump, Int. J. Refrig. 140 (2022) 103–111.
- [23] M. Ramirez, F.T. Kelly, J.L.C. Ciganda, J. Payá, A.H. Hassan, Experimental and numerical investigation of a novel high-temperature heat pump for sensible and latent heat delivery, Appl. Therm. Eng. (2024) 122961.
- [24] T. Ahmad, H. Chen, J. Shair, Water source heat pump energy demand prognosticate using disparate data-mining based approaches, Energy 152 (2018) 788–803.
- [25] F. Guo, Z. Chen, F. Xiao, A. Li, J. Shi, Real-time energy performance benchmarking of electric vehicle air conditioning systems using adaptive neural network and Gaussian process regression. Appl. Therm. Eng. 222 (2023) 119931.
- [26] FUSE FUll scale industrial heat pump using natural refrigerants, 2024, https://ispt.eu/projects/fuse/. (Accessed 26 March 2024).
- [27] Mayekawa Europe, 2024, http://www.mayekawa.eu/. (Accessed 26 March 2024).
- [28] Carnot lab accelerates sustainable industry, 2024, https://www.tno.nl/en/technology-science/labs/carnot-lab. (Accessed 26 March 2024).
- [29] MYCOM global, 2024, https://mayekawa.com/. (Accessed 26 March 2024).
- [30] J. Wang, An intuitive tutorial to Gaussian process regression, Comput. Sci. Eng. 25 (04) (2023) 4–11.
- [31] C.E. Rasmussen, C.K.I. Williams, Gaussian Processes for Machine Learning, MIT Press, ISBN: 026218253X, 2006.
- [32] A.C. Ispir, K. Zdybał, B.H. Saracoglu, T. Magin, A. Parente, A. Coussement, Reduced-order modeling of supersonic fuel-air mixing in a multi-strut injection scramjet engine using machine learning techniques, Acta Astronaut. 202 (2023) 564–584.
- [33] I.H. Bell, J. Wronski, S. Quoilin, V. Lemort, Pure and pseudo-pure fluid thermophysical property evaluation and the open-source thermophysical property library CoolProp, Ind. Eng. Chem. Res. 53 (6) (2014) 2498–2508.
- [34] U.D. of Energy, Furnaces and boilers, 2025, URL https://www.energy.gov/energysaver/furnaces-and-boilers. (Accessed 15 January 2025) (n.d.).
- [35] K.R. Wheeler, Efficient Operation of Diesel Generator Sets in Remote Conditions (Ph.D. thesis), Virginia Tech, 2017.

- [36] A. Marina, S. Spoelstra, H.A. Zondag, A. Wemmers, An estimation of the European industrial heat pump market potential, Renew. Sustain. Energy Rev. 139 (2021) 110545.
- [37] B. Zühlsdorf, High-temperature heat pumps: Task 1-technologies. Annex 58 about high-temperature heat pump, 2023.
- [38] CO2 emissions fee increase, 2024, URL https://business.gov.nl/amendment/co2-emissions-fee-increase/. (Accessed 28 June 2024).
- [39] Electricity industrial prices, 2024, URL https://www.globalpetrolprices.com/ map/electricity_industrial/. (Accessed 28 June 2024).
- [40] LPG prices, 2024, URL https://www.globalpetrolprices.com/map/lpg/. (Accessed 28 June 2024).
- [41] CO2 emission factors for fossil fuels, 2024, URL https://www.engineeringtoolbox. com/co2-emission-fuels-d 1085.html. (Accessed 28 June 2024).
- [42] The Netherlands, 2024, URL https://www.iea.org/countries/the-netherlands. (Accessed 28 June 2024).

- [43] Oil and petroleum products FAQs, 2024, URL https://www.eia.gov/tools/faqs/faq.php?id=74&t=11. (Accessed 28 June 2024).
- [44] N. Baek, U. Shin, J. Yoon, A study on the design and analysis of a heat pump heating system using wastewater as a heat source, Sol. Energy 78 (3) (2005) 427–440.
- [45] C. Arpagaus, F. Bless, M. Uhlmann, J. Schiffmann, S.S. Bertsch, High temperature heat pumps: Market overview, state of the art, research status, refrigerants, and application potentials, Energy 152 (2018) 985–1010.
- [46] D. Van de Bor, C.I. Ferreira, A.A. Kiss, Low grade waste heat recovery using heat pumps and power cycles, Energy 89 (2015) 864–873.
- [47] B. Hu, H. Liu, R. Wang, H. Li, Z. Zhang, S. Wang, A high-efficient centrifugal heat pump with industrial waste heat recovery for district heating, Appl. Therm. Eng. 125 (2017) 359–365.